Non-reciprocal phase shift induced by an effective magnetic flux for light

Lawrence D. Tzuang[1], Kejie Fang[2,3], Paulo Nussenzveig[1,4], Shanhui Fan[2] and Michal Lipson[1,5]★

Photons are neutral particles that do not interact directly with a magnetic field. However, recent theoretical work[1,2] has shown that an effective magnetic field for photons can exist if the phase of light changes with its direction of propagation. This direction-dependent phase indicates the presence of an effective magnetic field, as shown experimentally for electrons in the Aharonov–Bohm experiment. Here, we replicate this experiment using photons. To create this effective magnetic field we construct an on-chip silicon-based Ramsey-type interferometer[3–7]. This interferometer has been traditionally used to probe the phase of atomic states and here we apply it to probe the phase of photonic states. We experimentally observe an effective magnetic flux between 0 and 2π corresponding to a non-reciprocal 2π phase shift with an interferometer length of 8.35 mm and an interference-fringe extinction ratio of 2.4 dB. This non-reciprocal phase is comparable to those of common monolithically integrated magneto-optical materials.

The interaction of light and a magnetic field would enable new physical phenomena for photons, such as bending the direction of light and one-way edge modes[1,2]. Because photons are neutral particles, their interaction with a magnetic field relies on using magneto-optical materials. Recently, there have been demonstrations of on-chip isolators[8–10] and topologically protected edge modes[11–15] based on magneto-optical materials. However, magneto-optical materials are difficult to integrate on-chip and the magneto-optic effect is weak in the near-infrared and visible domains. Isolator schemes using dynamic modulation instead of magneto-optical materials have been demonstrated in optical fibres[16] and more recently in on-chip silicon and InP waveguides[17–19]. However, these works do not demonstrate an effective magnetic field. This leads to the fundamental question of whether one can generate an effective magnetic field directly coupled with photons in the optical domain while not being limited to the use of magneto-optical materials.

As shown by Fang et al.[1,2], an effective magnetic field for photons could be created if one could break the reciprocity of light such that its phase depends on its propagation direction. The link between the magnetic field **B** (and its associated gauge potential, **A**) and the direction-dependent phase is equivalent to the Aharonov–Bohm effect[20] for electrons, where the electrons acquire a direction-dependent phase ($\phi = (e/h) \int_r^{r'} \mathbf{A} \cdot \mathrm{d}\hat{r}$, where $B = \nabla \times \mathbf{A}$, e is the unit charge and h is Planck's constant) in the presence of a magnetic field. Recently, the effective magnetic field for radiofrequency photons was observed using a photonic Aharonov–Bohm interferometer[21]. The demonstration of such an effect in the on-chip optical domain provides a new functionality for on-chip light manipulation.

Here, we probe the phase of light using a Ramsey-type interferometer[3–7]. The basic form of a Ramsey-type interferometer is shown in Fig. 1a. In an atomic Ramsey interferometer, as an atom in the ground state enters the interferometer, the first laser (left) interacts with it, and the atomic state is rendered in a linear superposition of the ground and excited state. These two states have different propagation phases ($\Delta\phi_a$, due to rotation and gravitation, for example). A second laser excitation, in phase with the first, again transforms the atomic ground and excited states into linear superpositions. Thus, the probability of finding an atom exiting the interferometer in the ground state exhibits an interference profile depending on $\cos(\Delta\phi_a)$. In a photonic Ramsey interferometer (Fig. 1b), we replace the two atomic states and laser excitations with two photonic states (in our case even and odd modes in a waveguide; see later) and modulators, respectively. As light in the even mode (ground state) enters the interferometer, the first modulator (left) induces a refractive index perturbation and couples a portion of light in the even mode to the odd mode (excited state). Note that this transition is classical, in contrast to the atomic Ramsey interferometer. Following excitation (that is, coupling), similar to the atomic case, the propagating light is in a superposition of the even and odd modes. The two modes experience different phases
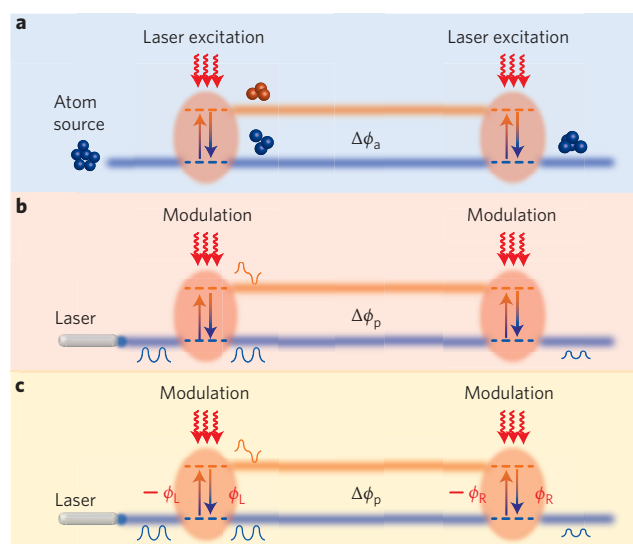

Figure 1 | Effective magnetic field for light using a Ramsey-type interferometer. a, Atomic Ramsey interferometer. **b**, Photonic Ramsey interferometer. **c**, Photonic Ramsey interferometer where the two modulators have different phases ϕ_L and ϕ_R.

[1]School of Electrical and Computer Engineering, Cornell University, Ithaca, New York 14853, USA, [2]Department of Electrical Engineering, Stanford University, Stanford, California 94305, USA, [3]Thomas J. Watson, Sr, Laboratory of Applied Physics, California Institute of Technology, Pasadena, California 91125, USA, [4]Instituto de Física, Universidade de São Paulo, PO Box 66318, 05315-970 São Paulo, Brazil, [5]Kavli Institute at Cornell for Nanoscale Science, Cornell University, Ithaca, New York 14853, USA. *e-mail: ml292@cornell.edu

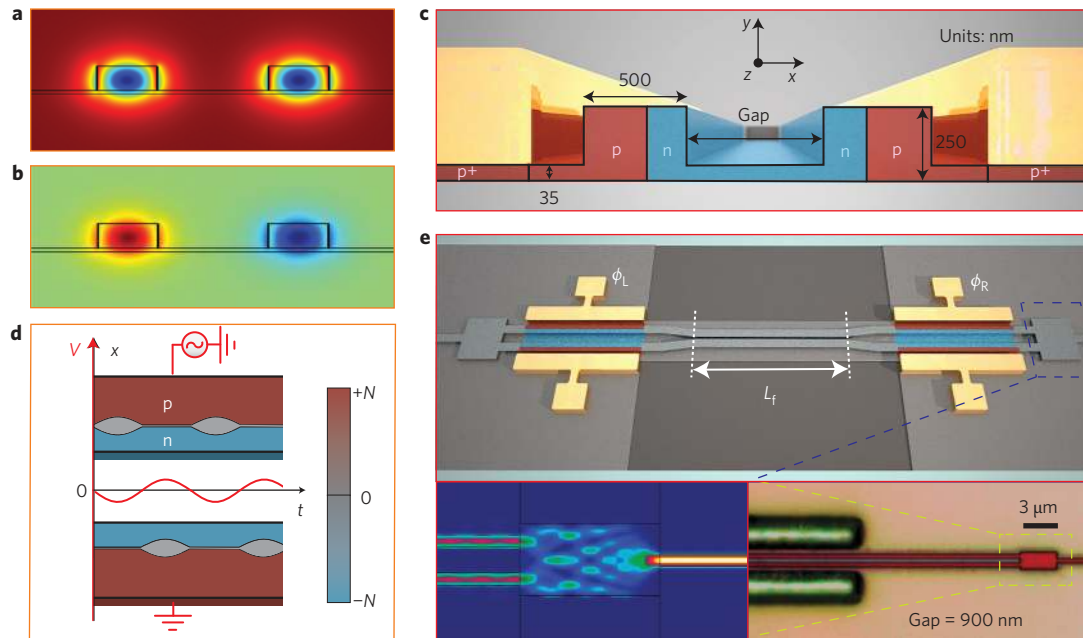**Figure 2 | Ramsey-type interferometer design and fabrication. a,b,** Simulated mode profiles for both the even mode (**a**) and the odd mode (**b**), which coexist in a silicon coupled waveguide structure. **c,** Cross-sectional view of the coupled waveguides. A set of pn and np diodes is doped to modulate the refractive index. **d,** Top view of carrier density (*N*) distribution in the coupled waveguide along the *x*-axis (slab omitted). The width of the depletion region (grey) changes over time as a sinusoidal signal is applied to the diodes. The applied sinusoidal voltage *V* is shown in red. **e,** A photonic Ramsey interferometer implemented as a silicon coupled-waveguide structure. Bottom: microscope image and simulated light transmission of a pair of multimode interference devices located at the outer ends of the interferometer.

($\Delta\phi_p$) because of their different propagation constants. A second modulator (right) couples light in the odd mode back into the even mode, and light exiting the interferometer exhibits an interference profile, as in the atomic version but now depending on cos($\Delta\phi_p$).

We use the Ramsey-type interferometer to probe the phase and break the reciprocity of light, thus inducing an effective magnetic field. This is achieved if the two modulators have different phases ϕ_L and ϕ_R (Fig. 1c). When inducing couplings, modulators impart their phases on photons. With respect to the phase of the local oscillator that drives the modulator, the imparted phase on photons is negative (positive) if excitation (de-excitation) occurs[1]. If the phases of both modulators are identical (Fig. 1b), then the total imparted phases are cancelled. However, if the modulators have different phases (Fig. 1c), these imparted phases are detected and the transmission becomes direction dependent. When light enters the interferometer from the left (right), the output of the interferometer is proportional to cos($\Delta\phi_p - \phi_L + \phi_R$) (cos($\Delta\phi_p - \phi_R + \phi_L$)). The non-reciprocal transmission is a result of an effective magnetic flux, where $B_{flux} = \phi_L - \phi_R$ (ref. 1). We implement the photonic Ramsey-type interferometer by using the supermodes (even and odd modes) of a silicon coupled-waveguides structure. The mode profiles are shown in Fig. 2a,b and the dimensions of the structure in Fig. 2c. The modulators are formed by embedding pn and np diodes in the waveguides (Fig. 2c). Figure 2d presents a top view of the carrier distribution under an applied sinusoidal voltage (red). The width of the depletion region (grey) changes as the signal is applied, which induces a change in the refractive index of the coupled waveguides[22,23]. The pn–np configuration[18] ensures that, at any instant in time, only one side of the coupled waveguides experiences a depletion width change, which enables coupling between the supermodes. Figure 2e presents an overview of the interferometer. The two modulators are identical and only their modulation phases are different (ϕ_R and ϕ_L). The length of each modulator is 3.9 mm, which in simulation provides an equal probability (50%) of populating both the two supermodes. The gap of the

coupled waveguides varies along the interferometer. At the edges where the modulators are located, this gap is 900 nm (to separate the two supermodes in frequency by a few GHz in the optical c-band; Supplementary Fig. 1). In the centre, the gap tapers (taper length of 100 μm) down to 550 nm and remains at this for a distance L_f such that the two supermodes experience different effective indices Δn_{eff}, and the phase difference between the two supermodes becomes $\Delta k \times L_f$ ($\Delta k = 2\pi\Delta n_{eff}/\lambda$ and λ is the optical wavelength). Here, L_f varies from 175 μm to 350 μm for different fabricated devices. We also place multimode interference devices at each end of the interferometer so that only the even mode enters and exits the interferometer. A microscope image and a simulated power distribution of the multimode interference are shown in Fig. 2e (bottom images).

We experimentally observed non-reciprocal fringe patterns, indicating the existence of an effective magnetic flux from 0 to 2π corresponding to a non-reciprocal 2π phase shift of 8.35 mm (length of our interferometer) and a fringe extinction ratio of 2.4 dB. Figure 3a shows the optical transmission of our devices when light is propagating from left to right (L → R) and right to left (R → L). Two synchronized sinusoidal radiofrequency signals are applied such that ϕ_L and ϕ_R are correlated. We chose $\lambda = 1,570$ nm to match the modulation frequency ($f_M = 4$ GHz) to the frequency difference between the supermodes. As shown in Fig. 3a we see full periods of sinusoidal optical transmissions (fringe patterns) as $\Delta\phi$ ($= \phi_L - \phi_R$) varies from 0 to 2π. The solid curves in Fig. 3a are the theory curve fits (Supplementary Section II), all of which match the experiments well. For all values of L_f we observe clear non-reciprocal transmission, where the $\Delta\phi$ that corresponds to the maximum transmission for R → L ($\Delta\phi_{R\rightarrow L}$) is different from that for L → R ($\Delta\phi_{L\rightarrow R}$). Figure 3b also shows a linear relationship between $|\Delta\phi_{R\rightarrow L} - \Delta\phi_{L\rightarrow R}|$ and L_f. This result is expected, because $\Delta\phi_{R\rightarrow L}$ and $\Delta\phi_{L\rightarrow R}$ are both proportional to the phase difference between the two supermodes, which is also proportional to L_f. The experiments (circles) match the theory well (solid line), and the data all
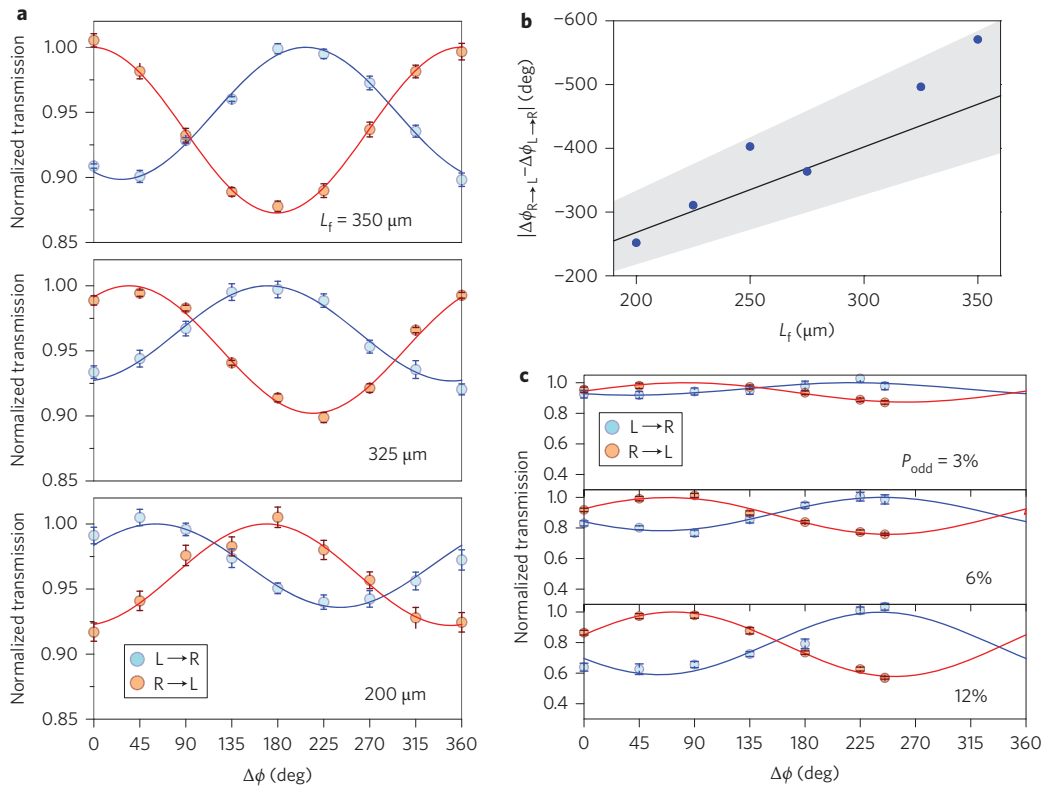
Figure 3 | Effective magnetic field experiment. a, Examples of measured (circles, normalized to the maximum curve fitted value) and theoretically fitted (solid lines) optical transmission for light travelling from left to right (L → R, blue) and right to left (R → L, red) for devices with different L_f, as a function of the phase difference between the two signals applied to the modulators ($\Delta\phi = \phi_L - \phi_R$). Wavelength = 1,570 nm; applied radiofrequency power = 24 dBm. Error bars represent one standard deviation from the measurement mean resulting from optical alignment fluctuations. **b**, Measured (circles) and theoretical (solid) difference $\Delta\phi$ when the transmission is maximum for L → R ($\Delta\phi_{L\to R}$) and R → L ($\Delta\phi_{R\to L}$) versus L_f. The grey region indicates the error of the theoretical curve when a 5% process variation is introduced. **c**, Measured and theoretically fitted optical transmission for light travelling from left to right (blue) and right to left (red) for $L_f = 350$ μm with increased population in the odd mode P_{odd} (shown as percentages) achieved by increasing the applied radiofrequency power.
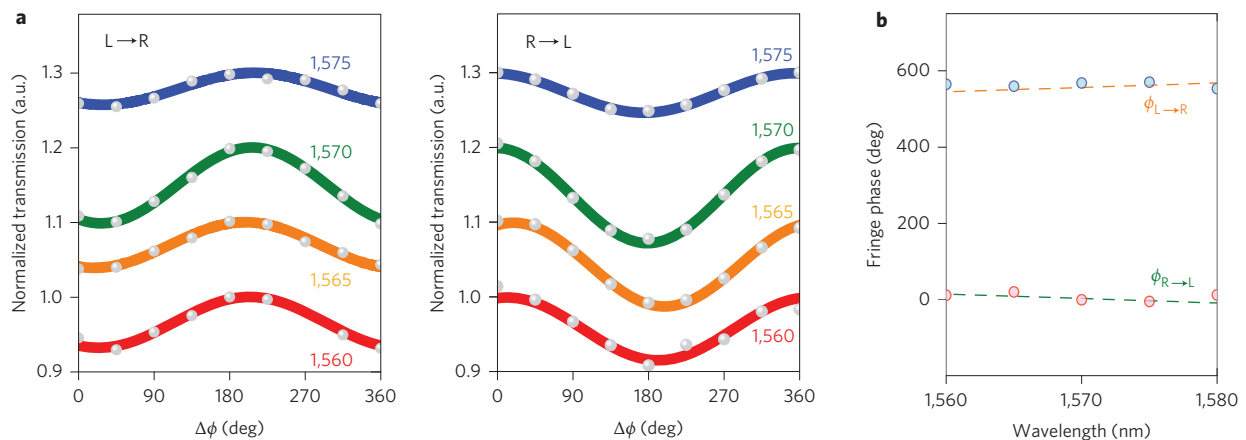

Figure 4 | Wavelength dependence of the interference effect for the photonic Ramsey-type interferometer. a, Measured (grey circles, normalized to the maximum curve fitted value) and theoretically fitted (solid lines) optical transmission of light travelling from left to right (L → R) and from right to left (R → L) versus $\Delta\phi$ for different laser wavelengths (1,560, 1,565, 1,570 and 1,575 nm) with $L_f = 350$ μm. **b**, Theoretical (dashed lines) and measured (circles) phase of the fringes for L → R and R → L versus wavelength.

lie within the theoretical window (grey) that accounts for ±5% process variation (related to slab thickness and the gap of the coupled waveguides). Figure 3c shows the transmission extinction ratios for light propagating from left to right (L → R) and right to left (R → L) with increased coupling between the even and odd

modes, achieved by increasing the applied radiofrequency power. As the power increases, the extinction ratio for $L_f = 325$ μm increases from 0.6 dB to 2.4 dB, corresponding to the population in the odd mode increasing from 3% to 12%. From these measurements we estimate that the power necessary to achieve maximum extinction

(that is, 50% population in the odd mode) is at least an order of magnitude larger than the theoretical value of 160 mW. This high power requirement in our experiments is due to both the RC cutoff (because the RC bandwidth of our device is ~2.5 GHz, smaller than the modulation frequency of 4 GHz) and the inefficiency of our pn diodes (we estimate our pn diodes to have only ~28% the efficiency of our designed value; for details see Supplementary Fig. 5). In principle, redesigning the dispersion of the coupled waveguides to operate at lower radiofrequencies, optimizing the diode profile[24] and increasing the length of the modulator should further increase the extinction ratio.

To confirm that the non-reciprocal fringes result from the interference between the supermodes, we measured the fringes at different wavelengths for $L_f = 350$ μm, as shown in Fig. 4a. This wavelength dependence of the fringe extinction ratio is due to the dispersion of the two supermodes; the frequency difference between the supermodes perfectly matches f_M at $\lambda \approx 1{,}570$ nm and not at other wavelengths. In Fig. 4a we also observe a slight shift of these fringe phases as λ changes. This is expected, because Δn_{eff} is also wavelength dependent. Figure 4b plots the theoretical (dashed line) and measured (circles) wavelength dependence of $\Delta\phi_{L\to R}$ and $\Delta\phi_{R\to L}$ from 1,560 nm to 1,575 nm. It is clear that the experiments and theory agree well.

In summary, we have used a new photonic interferometer scheme to measure a non-reciprocal phase of light (0 to 2π) and to induce an effective magnetic field for light. This non-reciprocal 2π phase shift in our interferometer with a length of 8.35 mm is comparable to commonly used monolithically integrated magneto-optical materials such as polycrystalline YIG and Ce:YIG films[9]. The scheme we use here also quantifies the population of both photonic states. The materials and fabrication processes we use are fully CMOS compatible. The demonstration of an effective magnetic field in conjunction with recent theoretical predictions will enable the development of novel photonic devices, including isolators and topological insulators. We also expect this work to stimulate the exploration of physics and applications of effective gauge potentials and topological manipulation for photons[25–31], by demonstrating for the first time an effective gauge potential for photons that break reciprocity and time-reversal symmetry.

Methods

Device fabrication. The device was fabricated using a silicon-on-insulator wafer. maN-2403 photoresist was used to mask the waveguide pattern using electron-beam lithography (EBL), and the silicon was then etched to leave a 35 nm slab. After forming the waveguide, four individual EBL steps using polymethyl methacrylate photoresist masks were used to implant boron (p/p$^+$, $1 \times 10^{20}/8 \times 10^{17}$ cm^{-3}) and phosphorus (n/n$^+$, $1 \times 10^{20}/8 \times 10^{17}$ cm^{-3}) to form the doping profile shown in Fig. 2c. The dopants were then activated using a furnace and the rapid thermal anneal process. After dopant activation, the waveguides were clad with 950 nm plasma-enhanced chemical vapour deposited SiO$_2$. EBL was used to write the mask for the vias, followed by reactive-ion etching through the SiO$_2$. After etching, 80 nm MoSi$_2$ and 1.6 μm aluminium were deposited to form the electrical contact.

Measurement and experimental set-up. The two signals applied to each of the modulators were provided by two signal generators with the same frequency (4 GHz) to match the frequency separation of the even and odd modes at a wavelength of 1,570 nm. We chose 4 GHz as the operational frequency because both signal generators provide the maximum output at this frequency. The two signal generators, each set at 24 dBm, were synchronized to ensure a correlated phase, and for both signals, 1% of the radiofrequency power was dropped through a directional coupler into the oscilloscope. The correlated phases from the two signal generators were then monitored using the oscilloscope. For both signals, the remaining 99% of power was delivered to the corresponding high-speed radiofrequency probes that contact the device pads. For the optical set-up, light was coupled from a tunable laser into the waveguide through a lensed fibre, and light transmission through the device was coupled out through another lensed fibre. The output light was then collected by a photodetector. Forward and backward transmissions were measured by interchanging the fibre connectors connecting the laser and photodetector. An illustration of the testing set-up is provided in Supplementary Figs 3 and 6.

References

1. Fang, K., Yu, Z. & Fan, S. Photonic Aharonov–Bohm effect based on dynamic modulation. *Phys. Rev. Lett.* **108,** 153901 (2012).
2. Fang, K., Yu, Z. & Fan, S. Realizing effective magnetic field for photons by controlling the phase of dynamic modulation. *Nature Photon.* **6,** 782–787 (2012).
3. Ramsey, N. F. A new molecular beam resonance method. *Phys. Rev.* **76,** 996 (1949).
4. Ramsey, N. F. *Molecular Beams* (Oxford Univ. Press, 1963).
5. Bordé, C. J. Atomic interferometry with internal state labelling. *Phys. Lett. A* **140,** 10–12 (1989).
6. Ramsey, N. F. Experiments with separated oscillatory fields and hydrogen masers. *Rev. Mod. Phys.* **62,** 541–552 (1990).
7. Dubetsky, B. & Kasevich, M. A. Atom interferometer as a selective sensor of rotation or gravity. *Phys. Rev. A* **74,** 023615 (2006).
8. Shoji, Y., Mizumoto, T., Yokoi, H., Hsieh, I-W. & Osgood, R. M. Jr Magneto-optical isolator with silicon waveguides fabricated by direct bonding. *Appl. Phys. Lett.* **92,** 071117 (2008).
9. Bi, L. et al. On-chip optical isolation in monolithically integrated non-reciprocal optical resonators. *Nature Photon.* **5,** 758–762 (2011).
10. Tien, M.-C., Mizumoto, T., Pintus, P., Kromer, H. & Bowers, J. E. Silicon ring isolators with bonded nonreciprocal magneto-optic garnets. *Opt. Express* **19,** 11740–11745 (2011).
11. Haldane, F. D. M. & Raghu, S. Possible realization of directional optical waveguides in photonic crystals with broken time-reversal symmetry. *Phys. Rev. Lett.* **100,** 013904 (2008).
12. Wang, Z., Chong, Y. D., Joannopoulos, J. D. & Soljačić, M. Reflection-free one-way edge modes in a gyromagnetic photonic crystal. *Phys. Rev. Lett.* **100,** 013905 (2008).
13. Raghu, S. & Haldane, F. D. M. Analogs of quantum-Hall-effect edge states in photonic crystals. *Phys. Rev. A* **78,** 033834 (2008).
14. Wang, Z., Chong, Y., Joannopoulos, J. D. & Soljačić, M. Observation of unidirectional backscattering-immune topological electromagnetic states. *Nature* **461,** 772–775 (2009).
15. Poo, Y., Wu, R., Lin, Z., Yang, Y. & Chan, C. T. Experimental realization of self-guiding unidirectional electromagnetic edge states. *Phys. Rev. Lett.* **106,** 093903 (2011).
16. Hwang, I. K., Yun, S. H. & Kim, B. Y. All-fiber-optic nonreciprocal modulator. *Opt. Lett.* **22,** 507–509 (1997).
17. Doerr, C. R., Dupuis, N. & Zhang, L. Optical isolator using two tandem phase modulators. *Opt. Lett.* **36,** 4293–4295 (2011).
18. Lira, H., Yu, Z., Fan, S. & Lipson, M. Electrically driven nonreciprocity induced by interband photonic transition on a silicon chip. *Phys. Rev. Lett.* **109,** 033901 (2012).
19. Doerr, C. R., Chen, L. & Vermeulen, D. Silicon photonics broadband modulation-based isolator. *Opt. Express* **22,** 4493–4498 (2014).
20. Aharonov, Y. & Bohm, D. Significance of electromagnetic potentials in the quantum theory. *Phys. Rev.* **115,** 485–491 (1959).
21. Fang, K., Yu, Z. & Fan, S. Experimental demonstration of a photonic Aharonov–Bohm effect at radio frequencies. *Phys. Rev. B* **87,** 060301(R) (2013).
22. Soref, R. & Bennett, B. R. Electrooptical effects in silicon. *IEEE J. Quantum Electron.* **23,** 123–129 (1987).
23. Gardes, F. Y. et al. High-speed modulation of a compact silicon ring resonator based on a reverse-biased pn diode. *Opt. Express* **17,** 21986–21991 (2009).
24. Spector, S. J. et al. Operation and optimization of silicon-diode-based optical modulators. *IEEE J. Sel. Top. Quantum Electron.* **16,** 165–172 (2010).
25. Hafezi, M., Demler, E. A., Lukin, M. D. & Taylor, J. M. Robust optical delay lines with topological protection. *Nature Phys.* **7,** 907–912 (2011).
26. Umucalilar, R. O. & Carusotto, I. Artificial gauge field for photons in coupled cavity arrays. *Phys. Rev. A* **84,** 043804 (2011).
27. Rechtsman, M. C. et al. Photonic Floquet topological insulators. *Nature* **496,** 196–200 (2013).
28. Khanikaev, A. B. et al. Photonic topological insulators. *Nature Mater.* **12,** 233–239 (2013).
29. Liang, G. Q. & Chong, Y. D. Optical resonator analog of a two-dimensional topological insulator. *Phys. Rev. Lett.* **110,** 203904 (2013).
30. Longhi, S. Effective magnetic fields for photons in waveguide and coupled resonator lattices. *Opt. Lett.* **38,** 3570–3573 (2013).
31. Hafezi, M., Mittal, S., Fan, J., Migdall, A. & Taylor, J. M. Imaging topological edge states in silicon photonics. *Nature Photon.* **7,** 1001–1005 (2013).

Author contributions

L.D.T. performed the experiment. L.D.T. and K.F. designed the experiment and analysed the data. P.N., S.F. and M.L. supervised the project. L.D.T and M.L. prepared the manuscript. K.F., P.N. and S.F. edited the manuscript.

Additional information

Supplementary information is available in the online version of the paper. Reprints and permissions information is available online at www.nature.com/reprints. Correspondence and requests for materials should be addressed to M.L.

Competing financial interests

The authors declare no competing financial interests.